半导体超晶格／量子阱物理与光电子器件

讲习班教程

第二部分

1991年1月

广东广州

Semiconductor Quantum Well Lasers

Guo Changzhi （郭长志）

北京大学物理系，北京 100871

Abstract

Some brief historical notes of the main development, the physical theory of the device characteristics, including the wave guiding and modal behaviors, gain and emission spectra, the Auger recombinations, the strain effect, the dynamics, the phase-noise linewidth, the design principles for low threshold, high T_o, single mode, low noise, narrow linewidth, high speed, the state-of-the-arts, including the new advances, the yet unsolved problems, and the possible perspective views of the semiconductor QW lasers have been carefully discussed.

CONTENTS

IV. GAIN AND SPONTANEOUS EMISSION SPECTRA

A. Some theoretical background on optical transitions
A-1. Einstein's relations
A-2. Optical transition matrix element
A-3. Gain and spontaneous spectra in bulk GaAs

B. Optical transition in QW
B-1. Simple treatment
B-2. Anisotropy of the optical transition matrix element in QW
B-3. Spectral broadening by intraband relaxation
B-4. Spectral broadening by no-k-selection
B-5. Nonparabolicity of energy band
B-6. Bandgap renormalization from many-body interaction
B-7. Band-mixing effect in QW
B-8. Differential gain and its consequences
B-9. Strain effect on gain

V. Lasing threshold of QW lasers

A. Threshold relations in general
B. Routes to lowest threshold
C. Strain effect on threshold
D. Temperature effect on threshold

VI. Effect of quantization dimension

A. Density of states
B. Wave functions and quantum energy levels
C. Diploe moment
D. Linear gain
E. Threshold current
F. Temperature dependence

VII. Conclusion

A. State-of-the-arts
B. Perspective views

I. INTRODUCTION

Since the first observation of quantum-size effect (QSE) in quantum well (QW) structure consisting of alternating ultrathin layers of semiconductors GaAs and AlGaAs grown by molecular beam epitaxy (MBE) in 1974 and the first observation of optically pumped laser oscillation from this system at 15K in the next year, the technology and the theory of semiconductor QW lasers have been developed rapidly. But due to the failure of the MBE tech-nique to grow low lasing threshold devices and InGaAsP/InP system in 1970s, the liquid phase epitaxy (LPE) technique was improved and the metal organic chemical vapor deposition (MOCVD) technique was developed to grow first InGaAsP/InP current injected QW laser with threshold current density not quite lower than its ordinary DH counterpart at that time, and the second merit of the steplike density-of-state in QW laser——the high T_0 (i.e., the threshold current less sensitive to temperature) had been realized in the GaAs/AlGaAs system, though T_0 in the InGaAsP/InP system seemed not much improved until now due to the intrinsic Auger nonradia-tive recombinations active in this long wave length material sys-tem. After the key improvement of the MBE growth technique advan-ced by W.T. Tsang in the end of 70s, the QW lasers with extremely low threshold current density were grown at first by MBE in 1981, and then by MOCVD techniques in 1982, and the improved modulation speed and narrower linewidth were also observed at this period.

At this first decade, the anisotropy of the refractive index and the waveguiding in multi-quantum well (MQW) or superlattice (SL) structure, the carrier collection, the emission spectra and its red-shift relative to the effective bandgap or absorption edge, and other problems related to the design and understanding of the QW lasers were taken into account and made some progress. Since the detail observations of the gain spectra of the GaAs/ AlGaAs MQW structure made in 1983, many efforts have been made to improve the simple gain theory. Such as, the anisotropy of the optical transition matrix element by lowered symmetry group which may result in the dominant TE mode lasing; the intraband relaxa-tion by carrier-carrier and carrier-phonon scattering, etc., which may result in the round-shaped gain spectra with tailings; the non-k-selection in optical transition with impurity centers which may also result in the round-shaped gain spectra but with-out tailings; the energygap shrinkage due to many body effect which may result in the red-shift; the refined band theory con-cerning the non-parabolic correction or bandmixing effect for calculating more accurate wave functions and eigenvalues in any configuration of QW or SL structures, in which the bandmixing effect may not only result in the lift or modification of the selection rule based on the ordinary concept of the distinguish-able heavy hole and light hole bands as the bulk material in the simple band model of QW or LS, but also may result in the red-shift. The debating longitudinal optical (LO)-phonon-assisted laser operation mechanism proposed earlier by Holonyak et al to explain the red-shift seems to be contradictory to the recent experiments and likely to be abandoned. Though many other rea-sons, such as, the irregularity of the well width, the raise of the high energy tail in the spontaneous

emission spectra, etc., have been proposed recently, the real physical cause of the puzzling red-shift problem is now still not completely clear.

The fundamental understanding of the physics underlying QW lasers obtained has greatly promoted the opto-electronic device technology. Many such devices have been improved and renewed by using QW structures as their main parts or their auxiliary parts. The need for integrating optical and electrical devices of different materials together into a monolithic opto-electric circuit promotes the recent interesting on strained QW lasers. This may be a vivid field aimed at developing new generations of optical computers and optical communications. [1-1]-[1-10]

REFERENCES

[1-1] R. Dingle, Festköperprobleme XV (1975) 21-48.

[1-2] N. Holonyak, Jr., R. M. Kolbas, R. D. Dupuis, P. D. Dapkus, IEEE J. Quantum Electron., QE-16, No.2 (Feb. 1980) 170-186.

[1-3] L. J. van Ruyven, J. Lumin., 29 (1984) 123-161.

[1-4] W. T. Tsang, IEEE J. Quantum Electron., QE-20, No.10 (Oct. 1984) 1119-1131.

[1-5] L.C. Liu, A. Yariv, J. Lumin., 30 (1985) 551-561.

[1-6] Y. Arakawa, A. Yariv, IEEE J. Quantum Electron., QE-22,No.9 (Sept. 1986) 1887-1899.

[1-7] L. Esaki, IEEE J. Quantum Electron., QE-22, No.9(Sept.1980) 170-186.

[1-8] H. Okamoto, Japan.J.Appl.Phys., 26, No.3(Mar.1987) 315-330.

[1-9] W. T. Tsang, Semiconductors and semimetals, Vol. 24 (1987) 397-458.

[1-10] C. Z. Guo, 1989 Workshop on Semiconductor Laser Technology, International School of Lasers and Applications, March 31-April 9, 1990, Beijing.

II. QSE IN QW OR SL STRUCTURES

A. The confined states

It is well known in elementary quantum mechanics that when an electron is confined by potential barriers separated to each other by a length less than the de Broglie wavelength or the mean free path of the electron, its energy state in each well between two barriers will be quantized into discrete levels or narrow bands depending on the thicknesses of the barriers.

In semiconductor, the spatial periodic crystal potential of certain symmetry (e.g., T_d for GaAs) will change the free mass of electron m_o into a certain effective mass m_j, and change the energy of the electron into bands (conduction band $E_c(\underline{k})$, valence band $E_v(\underline{k})$, etc.) with a certain bandgap E_g. The difference be-tween the bandgaps of barrier layer and well layer dE_g will dis-tribute in the conduction band and valence band as dE_c and dE_v, respectively, with

$$dE_c + dE_v = dE_g \tag{2-1a}$$

In terms of the band offset parameters in the conduction band and valence band, b_c and b_v, with

$$b_c + b_v = 1 \tag{2-1b}$$

the depth of the quantum well (QW) or the height of the barrier in the conduction band and valence band will be respectively

$$V_{bc} = dE_c = b_c dE_g, \quad V_{bv} = dE_v = b_v dE_g \tag{2-1c}$$

The Schrödinger equation of an electron in a semiconductor QW will be

$$\{-[\hbar^2/(2m_j)]d^2\phi/dx^2 + V_j(x)\}\phi(x) = E_j\phi(x), \quad j=c,v \tag{2-2}$$

where $V_j(x)=0$ for $|x| < d_w/2$, and $V_j(x)=V_{bj}$ for $|x| > d_w/2$.

(i) $V_{bj} \rightarrow \infty$

In a semiconductor QW of infinite depth, the solution of the Schrödinger equation (2-2) will be

$$E_{jn}^{\infty} = E_{j1}^{\infty} n^2, \quad E_{j1}^{\infty} = [\hbar^2/(2m_j)](\pi/d_w)^2 \tag{2-3a}$$

$$\phi_{jn}^{\infty}(x) = A\sin(n\pi x/d_w) \quad \text{for} \quad |x| \le d_w/2 \tag{2-3b}$$

$$= 0 \quad \text{for} \quad |x| \ge d_w/2 \tag{2-3c}$$

as shown in Fig.2-1[1-11].

Fig.2-1 Some eigenvalues and wavefunctions of different quantum numbers (n, n') in an infinite QW. [1-11]

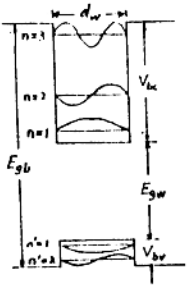

Fig. 2-1

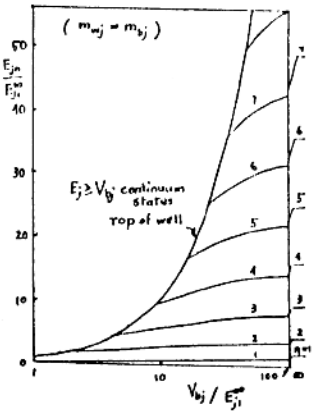

Fig. 2-2

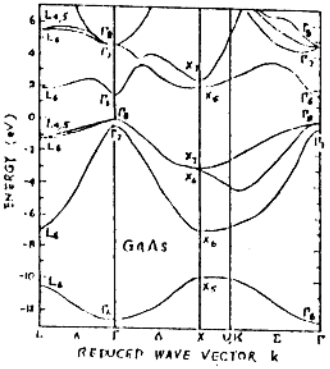

Fig. 2-3 (a)

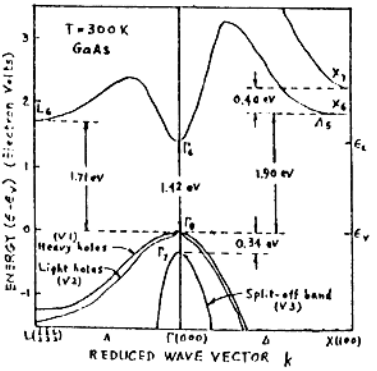

Fig. 2-3 (b)

(ii) $d_b \rightarrow \infty$

In the case of finite depth, the wavefunction of the Schrödinger equation (2-2) will be

$$\phi_{jn}(x) = A\cos(k_w x - n\pi/2) \qquad \text{for } |x| \le d_w/2 \qquad (2\text{-}4a)$$

$$= B\exp(-k_b|x|) \qquad \text{for } |x| \ge d_w/2 \qquad (2\text{-}4b)$$

The condition that the wavefunction ϕ_{jn} and the probability flux $(1/m_j)\{d\phi_{jn}/dx\}$ must be continuous at the boundaries between the well and barrier layers will lead to an eigenvalue equation:

$$\tan(k_w d_w/2 - n\pi/2) = k_b m_{wj}/(k_w m_{bj}) \qquad (2\text{-}5a)$$

$$k_w = (2m_{wj}E_{jn})^{1/2}/\hbar \ , \quad k_b = [2m_{bj}(E_{jn} - V_{bj})]^{1/2}/\hbar \qquad (2\text{-}5b)$$

The eigenvalue E_{jn} as a function of the well depth V_{bj} given by the solutions of eq.(2-5) are shown in Fig.2-2 [1-1] with both

| Fig.2-2 The energy levels E_{jn} of an electron in a QW of depth V_{bj} [1-1] with both normalized by E_{j1}^{∞} and with $m_{wj} = m_{bj}$. |

normalized by E_{j1}^{∞} and with $m_{wj} = m_{bj}$. For bulk III-V compound, such as GaAs, there are Γ-valley, L-valley (with 8th order degen-eracy), X-valley (with 6th order degeneracy) in conduction band; heavy-hole-band, light-hole-band, and spin-orbital-splitting-hole-band in valence bands as shown in Fig.2-3 [2-1]. The calcu-lated variations of the confined energy level E_{jn} with the well

| Fig.2-3 The band structure of bulk GaAs.[2-1] |

width d_w in SQW of this system for different band offset b_c are shown in Fig.2-4 [2-3].

| Fig.2-4 The variations of the energy level E_{jn} with the well width d_w in SQW for $\bar{x}$=.3 and (a) $V_{bj} = \infty$; (b) $b_c = 0.85$; (c) $b_c = 0.67$; (d) $b_c = 0.60$. [2-3] |

It can be seen that both the energy location of each quantized confined state and their separation increase with increasing V_{bj} and the energy levels higher than V_{bj} have been cutoff. The band parameters of bulk $GaAs/Al_xGa_{1-x}As$ system used in calculation are [2-1,2]:

$$\text{bandgap(eV):} \quad E_g^{\Gamma} = 1.424 + 1.247\bar{x} \qquad (0 \le \bar{x} \le .45)$$
$$= 1.424 + 1.427\bar{x} + 1.147(\bar{x}-.45)^2 \qquad (.45 \le \bar{x} \le 1)$$
$$E_g^{L} = 1.708 + .642\bar{x}$$
$$E_g^{X} = 1.900 + .125\bar{x} + .143\bar{x}^2$$
$$\Delta_s = 0.34 \qquad (2\text{-}6a)$$

$$\text{effective mass:} \quad m_c^{\Gamma} = (.0665 + .083\bar{x})m_0$$

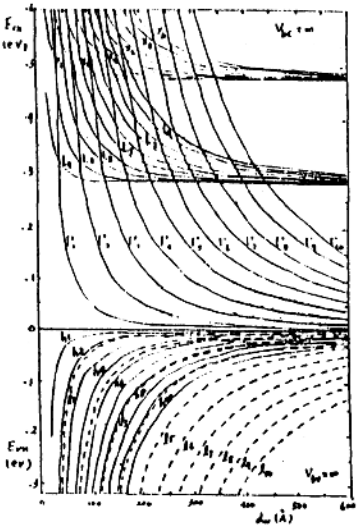

Fig. 2-4(a)

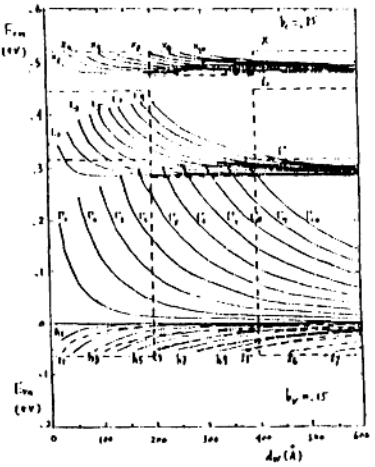

Fig. 2-4(b)

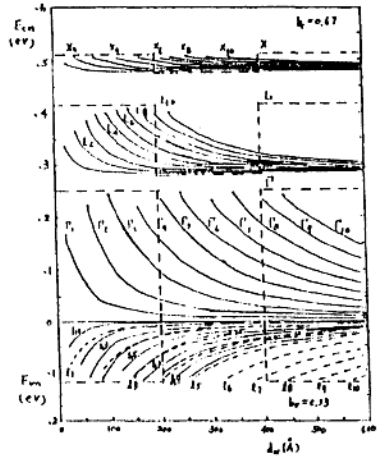

Fig. 2-4(c)

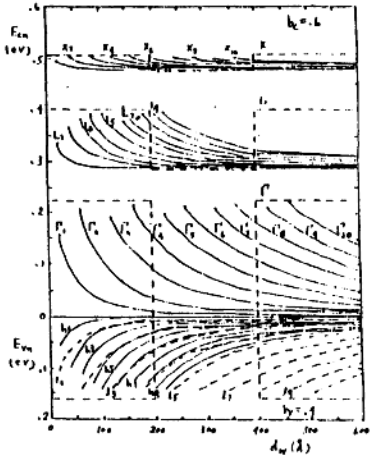

Fig. 2-4(d)

$$m_{c_\Gamma}^{L} = (.55 + .12\bar{x})m_o$$
$$m_c^{X} = (.85 - .07\bar{x})m_o$$
$$m_{hh} = (.45 + .302\bar{x})m_o$$
$$m_{lh} = (.082 + .057\bar{x})m_o$$
$$m_{sh} = (.15 + .09\bar{x})m_o \qquad (2\text{-}6b)$$

refractive index: $\bar{n}(\bar{x}) = 3.590 - .710\bar{x} + .091\bar{x}^2$ (2-6c)

(iii) Number of wells $N_w \to \infty$

In the case of MQW (with larger d_b) or SL (with smaller d_b) consisting of so many wells that it can be treated as an infinitely periodic structure (Fig.2-5), then

| Fig.2-5 The potential energy diagrams in (a) MQW and (b) SL structures. |

$$V(x + d) = V(x), \quad d = d_w + d_b \qquad (2\text{-}7a)$$

$$\phi(x) = u_k(x)\exp(ikx) \qquad (2\text{-}7b)$$

For $0 < x < d_w$, $V(x)=0$, $m_j=m_w$, $k_w = (2m_wE)^{1/2}/\hbar$, eq.(2-2) becomes

$$d^2u_k(x)/dx^2 + 2ik[du_k(x)/dx] + (k_w^2 - k^2)u_k(x)=0 \qquad (2\text{-}8a)$$

$$u_k(x) = A_o\exp[i(k_w-k)x] + B_o\exp[-i(k_w+k)x] \qquad (2\text{-}8b)$$

For $-d_b \le x < 0$, $V(x) = V_b$, $m_j = m_b$, $k_b = [2m_b(E-V_b)]^{1/2}/\hbar$, eq. (2-2) becomes

$$d^2u_k(x)/dx^2 + 2ik[du_k(x)/dx] - (k_b^2 - k^2)u_k(x) = 0 \qquad (2\text{-}9a)$$

$$u_k(x) = C_o\exp[(k_b-ik)x] + D_o\exp[-(k_w+ik)x] \qquad (2\text{-}9b)$$

By the condition that $u_k(x)$ and $(1/m_j)[du_k(x)/dx]$ must be continuous at $x = 0$ and at $x = d_w$ or $-d_b$, the eigenvalue equation for solving E will be

$$\cos(k_wd_w)\mathrm{ch}(k_bd_b) + \frac{k_bm_w - k_wm_b}{2k_bm_wk_wm_b}\sin(k_wd_w)\mathrm{sh}(k_bd_b) = \cos(kd) \qquad (2\text{-}10)$$

As $|\cos(kd)| \le 1$, the solution of eq.(2-10) at $\cos(kd) = +1$ will correspond to the lower bound of the subband splitted by the coupling between neighboring wells, and that at $\cos(kd) = -1$ will correspond to the upper bound. The variations of the subband width in a MQW with the barrier layer width d_b for $\bar{x}=.2$ and dif-ferent well width (d_w=40, 80 Å) are shown in Fig.2-6 [2-4] using

| Fig.2-6 The variations of the splitting of subbands in MQW for $\bar{x}$=.2, b_c=.85 of d_w=40 and 80 Å. [2-4] |

the same bulk parameters as in Fig.2-4. It can be seen that the subband splits at smaller barrier width, and the critical barrier

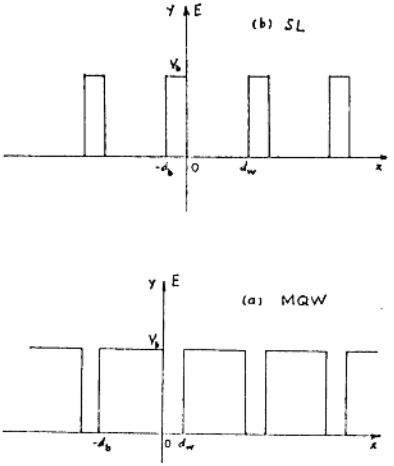
(b) SL
y
E
V_b
$-d_b$
0
d_w
x
(a) MQW
y
E
V_b
$-d_b$
0
d_w
x

Fig. 2-5

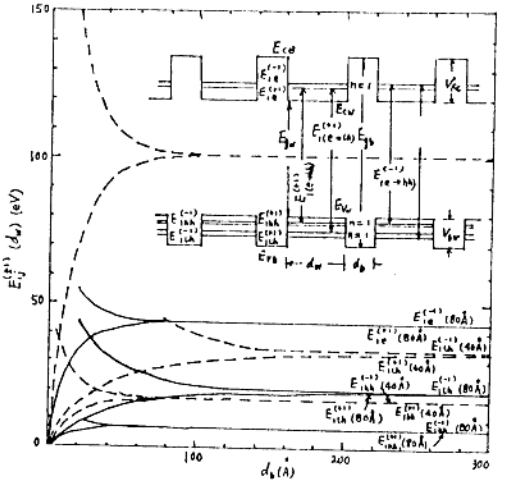
150
100
50
0
E_{ce}
E_{cw}
E_{fw}
E_{fb}
E_{vw}
E_{vb}
V_{ce}
V_{vw}
n=1
d_w
d_b
$E_{ij}^{(n)}$ (d_w) (eV)
$E_{1e}^{(-1)}$ (80Å)
$E_{1e}^{(+1)}$ (80Å)
$E_{1lh}^{(-1)}$ (40Å)
$E_{1lh}^{(+1)}$ (40Å)
$E_{1lh}^{(-1)}$ (40Å)
$E_{1lh}^{(-1)}$ (80Å)
$E_{1lh}^{(-1)}$ (80Å)
$E_{1hh}^{(+1)}$ (40Å)
$E_{1hh}^{(+1)}$ (80Å)
100
200
300
d_b(Å)

Fig. 2-6

width d_{bc} needed to split the subband increases from heavy hole, electron, to light hole in order. This is due to the coupling or tunnelling between neighboring wells increases when the effective mass m_b, the barrier width d_b, or the barrier height V_b decreas-es, or all decrease [cf. eq.(3-57d)].

B. Density of states (DOS) in QW

The allowable electron states or quantum states in a bulk crystal of finite volume with lengths L_x, L_y and L_z along x-, y- and z-axis, respectively, will separate in wave number space or k-space, $k = 2\pi/\lambda_o$, λ_o is the lasing wavelength in vacuum, to each other by $2\pi/L_x$, $2\pi/L_y$ and $2\pi/L_z$, respectively, like standing optical wave. Thus its density of states (DOS) per unit volume will be

$$\rho^{(o)}(E_j) = \frac{2d^3\underline{k}_j}{(2\pi/L_x)(2\pi/L_y)(2\pi/L_z)} \cdot \frac{1}{L_xL_yL_z}$$

$$= [1/(2\pi^2)](2m_j/\hbar^2)^{3/2}(E_j)^{1/2} \qquad (2\text{-}11a)$$

for $E_j = \hbar^2k_j^2/(2m_j)$, so that

$$dE_j = (\hbar^2k_j/m_j)dk_j, \qquad k_j = (2m_jE_j)^{1/2}/\hbar \qquad (2\text{-}11b)$$

where

$$E_j = E_o - E_{jo}, \qquad k_j^2 = k_{jx}^2 + k_{jy}^2 + k_{jz}^2 \qquad (2\text{-}11c)$$

the two different spin states of electron have been taken into account in eq.(2-11a).

In QW, the x-component of the wave number vector of electron k_{jx} is confined and quantized into discrete eigenvalues, so that only the other two components of the wave number vector k_{jy} and k_{jz}, can be treated as above. Thus

$$\rho^{(1)}(Ej) = \frac{2d^2\underline{k}_{j_t}}{(2\pi/L_y)(2\pi/L_z)} \cdot \frac{1}{L_xL_yL_z}$$

$$= m_j/(\pi\hbar^2L_x) \equiv \rho_{j1}, \qquad L_x = d_w \qquad (2\text{-}12a)$$

for $E_{j_t} = \hbar^2k_{j_t}^2/(2m_j)$, so that

$$dE_{j_t} = (\hbar^2k_{j_t}/m_j)dk_{j_t}, \qquad k_{j_t} = (2m_jE_{j_t})^{1/2}/\hbar \qquad (2\text{-}12b)$$

$$E_j = E_{jn} + E_{j_t}, \qquad k_{j_t}^2 = k_{jy}^2 + k_{jz}^2 \qquad (2\text{-}12c)$$

The relation between the DOS in QW, eq.(2-12a), and that in bulk, eq.(2-11a), is shown in Fig.2-7[2-3]. It can be seen that the DOS in QW coincides with that in bulk at $E_j = E_{jn}$; the DOS between E_{jn} and $E_{j(n+1)}$ is a constant equals to n times of ρ_{j1}; the DOS does not equal to 0 at $k_{j_t} = 0$.

| Fig.2-7 The density of states in QW and in bulk.[2-3] |

C. Populations on confined states

The population of electron on a confined state E_o in the conduction band is determined by the Fermi-Dirac (F-D) distribution function:

$$f_c(E_c) = 1/[1+\exp(\frac{E_o-F_{co}}{k_BT})] = 1/[1+\exp(\frac{E_c-F_c}{k_BT})] \quad (2\text{-}13a)$$

and that in the valence band is determined by:

$$f_v(E_v) = 1/[1+\exp(\frac{E_o-F_{vo}}{k_BT})] = 1/[1+\exp(\frac{F_v-E_v}{k_BT})] \quad (2\text{-}13b)$$

$$= 1 - f_h(E_v) \quad (2\text{-}13c)$$

the related energy scales are illustrated in Fig.2-8. The number

| Fig.2-8 The related energy scales used in the text. |

of electron per unit volume or the concentration of electron on the confined state in each band is given by integrating the product of the related DOS function and F-D function, and results in

Γ-band: $N^{\Gamma} = \sum_n N_n^{\Gamma}$ (2-14a)

$$N_n^{\Gamma} = \int_{-\infty}^{\infty} \rho_{cn}^{\Gamma}(E_c) f_c(E_c) dE_c = \frac{m_c^{\Gamma} k_B T}{\pi\hbar^2 d_w} \ln\{1+\exp[-(E_{cn}^{\Gamma}-F_c)/(k_BT)]\} \quad (2\text{-}14b)$$

L-band: $N^{L} = \sum_n N_n^{L}$ (2-15a)

$$N_n^{L} = \int_{-\infty}^{\infty} \rho_{cn}^{L}(E_c) f_c(E_c) dE_c = \frac{4m_c^{L} k_B T}{\pi\hbar^2 d_w} \ln\{1+\exp[-(E_{cn}^{L}-F_c)/(k_BT)]\} \quad (2\text{-}15b)$$

X-band: $N^{X} = \sum_n N_n^{X}$ (2-16a)

$$N_n^{X} = \int_{-\infty}^{\infty} \rho_{cn}^{X}(E_c) f_c(E_c) dE_c = \frac{3m_c^{X} k_B T}{\pi\hbar^2 d_w} \ln\{1+\exp[-(E_{cn}^{X}-F_c)/(k_BT)]\} \quad (2\text{-}16b)$$

Similarly, the concentrations of the heavy-hole (P^{hh}), light-hole (P^{lh}) and the spin-orbital-splitting-hole (P^{sh}) on the confined state in valence bands (Fig.2-3) are respectively:

hh-band: $P^{hh} = \sum_n P_n^{hh}$ (2-17a)

$$P_n^{hh} = \int_{-\infty}^{\infty} \rho_{vn}^{hh}(E_v)[1-f_v(E_v)]dE_v = \frac{m_{hh} k_B T}{\pi\hbar^2 d_w} \ln\{1+\exp[-(E_{vn}^{hh}-F_v)/(k_BT)]\} \quad (2\text{-}17b)$$

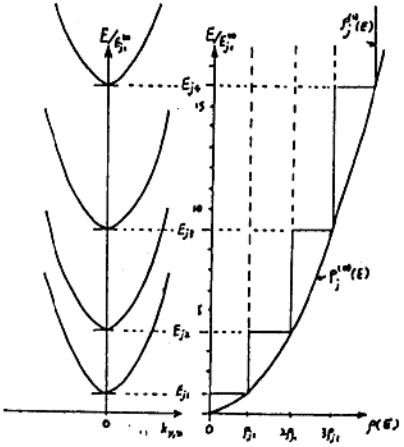

Fig. 2-7

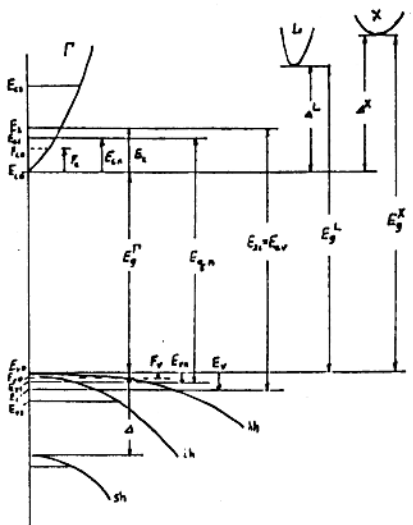

Fig. 2-8

lh-band: $P^{lh} = \Sigma_n P_n^{lh}$ (2-18a)

$$P_n^{lh} = \int_{-\infty}^{\infty} \rho_{vn}^{lh}(E_v)[1-f_v(E_v)]dE_v = \frac{m_{lh}k_BT}{\pi\hbar^2 d_w}\ln\{1+\exp[-(E_{vn}^{lh}-F_v)/(k_BT)]\} \quad (2-18b)$$

sh-band: $P^{sh} = \Sigma_n P_n^{sh}$ (2-19a)

$$P_n^{sh} = \int_{-\infty}^{\infty} \rho_{vn}^{sh}(E_v)[1-f_v(E_v)]dE_v = \frac{m_{sh}k_BT}{\pi\hbar^2 d_w}\ln\{1+\exp[-(E_{vn}^{sh}-F_v)/(k_BT)]\} \quad (2-19b)$$

The total concentrations of the electron (N) and hole (P) are respectively

$$N = N^{\Gamma} + N^{L} + N^{X}, \quad P = P^{hh} + P^{lh} + P^{sh} \quad (2-20a)$$

The related quasi-Fermi levels in conduction band (F_c) and in valence bands (F_v) are determined by eq.(1-20a) and the charge neutrality condition (in the case of no ionized impurity):

$$N = P \quad (2-20b)$$

The calculated populations on different confined states in the case of $GaAs/Al_xGa_{1-x}As$ SQW are shown in Fig.2-9 [2-3] using the same bulk parameters as in Fig.2-4. It can be seen that both

Fig.2-9 The populations of electron (N_n^j) and hole (P_n^j) and the related quasi-Fermi levels (F_c,F_v) as the functions of the well width d_w of a SQW for x=.3, $N = 3\times10^{18}$ cm^{-3} and (a)$V_b=\infty$; (b)b_c=.85; (c)b_c=.67; (d)b_c=.60. [2-3]

of the quasi-Fermi levels F_c and F_v are almost independent of the well width d_w and the difference between neighboring confined states increases with the decrease of the well width d_w.

D. The experimental verifications of QSE in semiconductor

The quantum size effect in semiconductor was conceived to be a way to realize quantum tunnelling and many other phenomena of both theoretical and technical interest by L. Esaki and R. Tsu of IBM Research Laboratory in 1969 [2-5]. The real existence of QSE in GaAs/AlGaAs system was firmly established by the following four earlier experimental observations:

(i) The resonant tunnelling in a double barrier structure consisting of GaAs/AlGaAs/GaAs/AlGaAs/GaAs layers grown by the then developed molecular beam epitaxy (MBE) technology was observed experimentally by L.L. Chang, L. Esaki, and R. Tsu in 1974 for the first time, as shown in Fig.2-10 [2-6].

Fig.2-10 The resonant tunnelling observed in GaAs/AlGaAs MQW. [2-6]

(ii) The exciton optical absorption spectra of MBE grown GaAs/

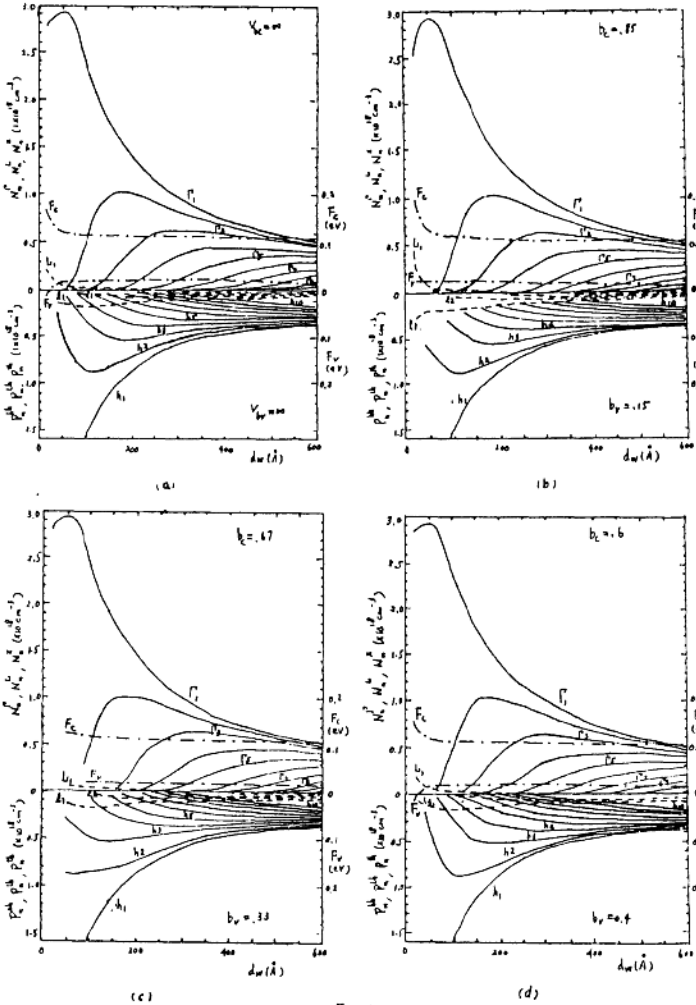

Fig. 2-9